828 *Biochemistry* **2011,** *50,* 828–835
DOI: 10.1021/bi1014002

BIOCHEMISTRY
including biophysical chemistry & molecular biology
Article

The Amyloid Precursor Protein C-Terminal Fragment C100 Occurs in Monomeric and Dimeric Stable Conformations and Binds γ-Secretase Modulators†

Anne Botev,‡ Lisa-Marie Munter,‡ Ringo Wenzel,§ Luise Richter,‡ Veit Althoff,‡ Jochen Ismer,∥ Ulla Gerling,‡ Christoph Weise,‡ Beate Koksch,‡ Peter W. Hildebrand,∥ Robert Bittl,§ and Gerd Multhaup*,‡

‡*Institut für Chemie und Biochemie, Freie Universität Berlin, Thielallee 63, 14195 Berlin, Germany,* §*Institut für Experimentalphysik, Freie Universität Berlin, Arnimallee 14, 14195 Berlin, Germany, and* ∥*Institut für Medizinische Physik und Biophysik, Charité Berlin, Ziegelstrasse 5-9, 10117 Berlin, Germany*

Received August 30, 2010; Revised Manuscript Received December 14, 2010

ABSTRACT: The amyloid-β (Aβ) peptide is contained within the C-terminal fragment (β-CTF) of the amyloid precursor protein (APP) and is intimately linked to Alzheimer's disease. *In vivo*, Aβ is generated by sequential cleavage of β-CTF within the γ-secretase module. To investigate γ-secretase function, *in vitro* assays are in widespread use which require a recombinant β-CTF substrate expressed in bacteria and purified from inclusion bodies, termed C100. So far, little is known about the conformation of C100 under different conditions of purification and refolding. Since C100 dimerization influences the efficiency and specificity of γ-secretase cleavage, it is also of great interest to determine the secondary structure and the oligomeric state of the synthetic substrate as well as the binding properties of small molecules named γ-secretase modulators (GSMs) which we could previously show to modulate APP transmembrane sequence interactions [Richter et al. (2010) *Proc. Natl. Acad. Sci. U.S.A. 107*, 14597−14602]. Here, we use circular dichroism and continuous-wave electron spin resonance measurements to show that C100 purified in a buffer containing SDS at micelle-forming concentrations adopts a highly stable α-helical conformation, in which it shows little tendency to aggregate or to form higher oligomers than dimers. By surface plasmon resonance analysis and molecular modeling we show that the GSM sulindac sulfide binds to C100 and has a preference for C100 dimers.

Recently, we and others have shown that the amyloid precursor protein (APP)[1] forms dimers via at least three dimerization sites, two different sites in the ectodomain (*1*, *2*) and a third dimerization site formed by three consecutive GxxxG motifs as part of the APP transmembrane sequence (APP-TMS) (*3*). Cleavage of APP by β-secretase yields the C-terminal fragment β-CTF or C100 (the terms β-CTF and C100 are used as synonyms). A subsequent cleavage of β-CTF by the γ-secretase complex is the crucial event in Alzheimer's disease that creates Aβ peptides. Dimerization of APP and especially of the γ-secretase substrate β-CTF is a risk factor for the formation of toxic Aβ42 (*1*, *3*, *4*).

Expression of C100 per se is not neurotoxic in a mouse model (*5*), and since C100 is a major substrate of the γ-secretase module, it constitutes a prime target for therapeutic intervention. C100 is the only known γ-secretase substrate comprising a GxxxG motif in triplicate, thus making dimerization of the APP-TMS unique (*3*, *6*). Mutational analysis revealed that a disruption of the dimer interface by glycine-to-alanine mutations at positions 29 and 33 of the Aβ sequence gradually attenuated the APP-TMS dimerization strength. By these mutations, the formation of Aβ42 was diminished in favor of Aβ38, whereas Aβ40 levels remained largely unaffected both for wild-type APP and for hereditary APP mutants (*3*, *7*). A subset of γ-secretase modulators (GSMs), including ibuprofen, indomethacin, and sulindac sulfide, known to effectively modulate the production of Aβ peptides *in vitro* and *in vivo*, decreasing Aβ42 levels in favor of increasing Aβ38 levels (*8*, *9*), was recently described to bind to the membrane-spanning Aβ sequence (*10*, *11*). Contrasting findings on the specificity of binding raised questions about the mechanism of GSM interaction with the amino acid sequence (*10*, *12*). Meanwhile, from surface plasmon resonance and NMR experiments it has been shown that GSMs bind to Aβ and that this interaction is mainly mediated by conformational characteristics like an α-helical flat protein surface (*11*).

As C100 is widely used in *in vitro* assays with the γ-secretase complex purified from eukaryotic cell membranes, it is highly desirable to know the exact conformation and the oligomeric state of the APP-derived β-CTF substrate produced in *Escherichia coli*. However, little is known about the oligomeric state of C100 when refolded in the presence of sodium dodecyl sulfate (SDS). Therefore, we performed a detailed structural study of C100 using circular dichroism (CD) and continuous-wave electron spin resonance (cw-ESR). We show that efficiently labeled C100 is neither particularly prone to aggregation nor to forming

†This work was supported by the Deutsche Forschungsgemeinschaft (DFG) through SFB 740 and Project HI 1502/1-1 (to P.W.H.) and by the Hans und Ilse Breuer Stiftung.

*Corresponding author: phone, +49 (0) 30 838 52905; fax, +49 (0) 30 838 56509; e-mail, multhaup@biochemie.fu-berlin.de.

[1]Abbreviations: Aβ, amyloid-β; APP, amyloid precursor protein; C100, 99-residue APP-CTF plus methionine; CD, circular dichroism; CTF, carboxy-terminal fragment; cw-ESR, continuous-wave electron spin resonance; DFDNB, 1,5-difluoro-2,4-dinitrobenzene; DMSO, dimethyl sulfoxide; DOC, sodium deoxycholate; *E. coli*, *Escherichia coli*; EDTA, ethylenediaminetetraacetic acid; GSM, γ-secretase modulator; IPTG, isopropyl β-D-1-thiogalactopyranoside; LMPG, lysomyristoylphosphatidylglycerol; MALDI-MS, matrix-assisted laser desorption/ionization mass spectrometry; MTSL, 1-oxy-2,2,5,5-tetramethylpyrroline-3-methyl methanethiosulfonate label; NMR, nuclear magnetic resonance; NTA, nitrilotriacetic acid; NP-40, Nonidet P-40; PAGE, polyacrylamide gel electrophoresis; SPR, surface plasmon resonance; TCEP, tris(2-carboxyethyl)phosphine; wt, wild type.

 Published on Web 12/27/2010

higher oligomers. We verified by CD measurements that C100 prepared in solutions containing SDS at micelle-forming concentrations has an α-helical, highly stable conformation. Surface plasmon resonance (SPR) analysis revealed that the GSM sulindac sulfide binds to C100 and that this interaction is impaired when residue glycine 33 within the Aβ sequence is changed into an isoleucine whereas sulindac sulfide preferentially binds to engineered C100 dimers.

METHODS

Mutagenesis, Overexpression, Purification, and Spin Labeling of APP-β-CTF (C100). The vector pQE60-C100 used for expression encodes for the 99 C-terminal amino acids of APP including the Aβ sequence and AICD as well as an additional N-terminal methionine and a C-terminal hexahistidine purification tag (His tag). Point mutations were generated at positions L17, F19, and G33 inside and S59 outside the Aβ region using site-directed mutagenesis, and amino acid substitutions were confirmed by DNA sequencing.

Lysogenic broth/0.1 mg/mL ampicillin was added to an overnight culture of *E. coli* XL1blue cells transformed with pQE60-C100, and cells were grown at 37 °C and 160 rpm (shaker) to an OD_{600} of ~0.5. C100 expression was induced by addition of 1 mM IPTG, and cells were harvested by centrifugation after 4 h of incubation. The cell pellets were stored at −20 °C.

Cell pellets were resuspended in TE buffer (20 mM Tris-HCl, 1 mM EDTA, pH 7.5) and disrupted by three passages through a French press. Inclusion bodies containing C100 were pelleted for 10 min at 25000*g* and 12 °C, and protein was dissolved in urea buffer (20 mM Tris-HCl, pH 8.5, 100 mM NaCl, 1 mM EDTA, 6 M urea, 1% Triton X-100, 1% SDS, 1 mM $CaCl_2$, 1× Complete protease inhibitor (Roche)) by sonication. The protein solution was centrifuged as before, and the supernatant was immediately diluted 1:4 with Tris/NaCl buffer (20 mM Tris-HCl, 50 mM NaCl, pH 7.5). Disulfide bonds were reduced overnight at 4 °C with 2.5 mM TCEP (Sigma), and the solution was further diluted 1:5 with Tris/NaCl buffer.

For purification and spin labeling of C100, the protein was incubated overnight with Ni-NTA agarose beads. The beads were washed with 40 column volumes of washing buffer (50 mM Tris-HCl, 300 mM NaCl, detergent (usually 0.3% SDS), pH 8.0) containing 0.02−0.2 mM TCEP. For spin labeling, the C100-loaded beads were incubated on a shaker for 2 h at room temperature and 800 rpm with 4 column volumes of washing buffer containing 0.02−0.2 mM TCEP and 0.8−1.6 μmol (10−20-fold molar excess) of the sulfhydryl reactive spin label MTSL (Toronto Research Chemicals) dissolved in 50% DMSO. For MTSL excess calculation, the C100 protein concentration was determined by RCDC protein assay (Bio-Rad Laboratories) according to the manufacturer's instructions after a test purification assuming a protein recovery rate of 100%. After labeling, the column was rinsed with 120 column volumes of washing buffer without TCEP, and C100 was eluted twice with 4 column volumes of elution buffer (washing buffer plus 50 mM EDTA, 0.02% NaN_3 and 1× Complete protease inhibitor) after 10 min of incubation at room temperature and 800 rpm. Samples were stored at 4 °C. To concentrate the samples and remove unbound MTSL from the eluates, 0.5 mg of C100 was washed on a 10 kDa cutoff Ultrafree-0.5 centrifugal filter device (Millipore, Billerica, MA) with 5 mL of washing buffer without detergent (for samples prepared in the presence of SDS) or with 0.1% sodium deoxycholate (DOC).

For analysis of purity and labeling efficiency, samples of washed and concentrated proteins were separated on a 15% SDS−PA gel, stained with Coomassie Brilliant Blue using GelCode Blue Safe Protein Stain (Thermo Scientific), and destained overnight in water. Usual working concentrations of C100 samples were between 50 and 300 μM.

Circular Dichroism (CD) Spectroscopy. For CD measurements, buffer was exchanged to 10 mM Tris/H_3PO_4 and 50 mM sodium phosphate, pH 8.0, or to cross-linking buffer by washing on a centrifugal filter device. Samples containing 50 μM C100 were measured on a Jasco J-810 spectropolarimeter at a path length of 0.2 mm at 20 °C, using 100 nm/min scanning speed, 1 s response time, and three scans per measurement. Buffer control was subtracted from each sample spectrum.

Continuous-Wave Electron Spin Resonance (cw-ESR) Spectroscopy. X-band cw-ESR measurements were performed on a home-built cw spectrometer, consisting of a Bruker ER 046 XK-T microwave bridge controlled by a Bruker ER 048 X Bridge controller. The magnet stems from an AEG 20 XT spectrometer system and is powered via a Bruker ER 081S power supply/Bruker B-H15 field controller setup. Signals are detected via a Stanford Research SR 810 DSP lock-in amplifier at 100 kHz modulation frequency, 2.7 G modulation amplitude, and a lock-in time constant of 100 ms. All measurements were done using a Bruker SHQ resonator at room temperature (296 K) and a microwave power of 2 mW (frequency = 9.38 GHz). Typical C100 concentrations measured were 50−300 μM.

Cross-Linking of C100. For C100 cross-linking, buffer was exchanged to 50 mM sodium phosphate (pH 8.0). C100 samples at 50 μM were incubated with a 5−50-fold molar excess of DFDNB (Thermo Fisher) dissolved in acetone or with the vehicle control. Cross-linking was performed for 30 min at room temperature and continued at 4 °C for 1−3 days. Samples were analyzed by SDS−PAGE and Coomassie Brilliant Blue staining, CD, and cw-ESR.

Surface Plasmon Resonance Analysis. SPR experiments were performed using a BIAcore 3000 instrument and NTA sensor chip (GE Healthcare). The sensor chip was charged with 20 μL of 500 μM $NiCl_2$ in eluent buffer (0.01 M HEPES, 0.15 M NaCl, 1 μM EDTA, 0.005% Tween 20, pH 7.4). The dispenser buffer consisted of eluent buffer with 3 mM EDTA. For C100 eluates from Ni-NTA columns (see above), buffer was exchanged to eluent buffer, and samples were diluted to concentrations of 0.125 μg/μL for C100 wt, 0.2 μg/μL for G33I, and 0.025 μg/μL for L17C. An aliquot (10 μL) of these samples was injected at a flow rate of 30 μL/min, yielding approximately equal response levels. For a negative control, C100 wt was injected onto a flow cell not charged with Ni, yielding no change in response units. Sulindac sulfide and sulindac sulfone (Sigma-Aldrich) 5, 10, 25, and 50 mM stock solutions in DMSO were diluted 1:1000 in eluent buffer, and 30 μL was injected at a flow rate of 30 μL/min. After a dissociation phase of 200 s the next injection followed immediately since response returned to baseline level due to fast GSM dissociation, and no regeneration step was required. C100 bound to Ni on the NTA sensor chip was stripped with two 1 min pulses of 30 μL of regeneration solution (eluent buffer with 0.35 M EDTA), and residual amounts of C100 precipitated on the sensor chip surface were removed by consecutive injections of 30 μL of 100 mM NaOH, 8 M urea, and 0.5% SDS and washing with eluent buffer overnight. Removal of C100 from the sensor chip surface was checked by injection of 30 μL of W0-2 antibody (The Genetics Co.) diluted in eluent buffer to 3.4 μg/mL.

Flexible Docking of Sulindac Sulfide to the APP-TMS wt and G33I Tertiary Structure Model. The APP-TMS model based on the tertiary structure of glycophorin A was used from previous analyses (*3*). The G33I mutant was built using the PyMOL Molecular Graphics System (http://www.pymol.org) and energetically minimized with GROMACS (http://www.gromacs.org/). Sulindac sulfide docking was performed as described previously (*11*).

RESULTS

Purification and Stability of C100 in Detergent-Containing Buffers. Single point mutations L17C, F19C, or G33I (according to Aβ numbering), the latter of which has been shown to attenuate noncovalently occurring dimerization (*3*), were introduced within the Aβ region by site-directed mutagenesis (Figure 1A). A C-terminal His tag enabled purification of C100 expressed in *E. coli* on a Ni-NTA column. To optimize the yield of C100, different concentrations of the detergents SDS, NP-40, and DOC were tested for the ability to solubilize C100 during affinity chromatography and prevent its aggregation. As exemplarily shown for the L17C mutant (Figure 1B), protein concentrations suitable for biophysical studies (see below) were obtained with SDS and DOC. After removal of precipitates by centrifugation, C100 eluted in the presence of NP-40 reached a maximum concentration of 30 μM. With DOC or SDS, C100 was eluted at a concentration of 120 μM. Further concentration on a centrifugal filter device yielded a stable protein solution of up to 300 μM in the presence of 0.3% SDS, while in DOC-containing buffer, the eluted sample could not be further concentrated without protein precipitation. Therefore, all further experiments were performed in the presence of 0.3% SDS. Under the conditions used the SDS concentration exceeds the micelle-forming concentration. Thus, the sustained solubility of C100 during the concentration step without additional SDS in the washing buffer is best explained by the insertion of C100 into detergent micelles.

Purified C100 was analyzed by CD measurement after removal of EDTA. The CD spectra revealed a predominantly α-helical conformation, as is visible in the spectra of C100 F19C eluted from the Ni-NTA column (Figure 1C). C100 F19C prepared in the presence of 0.1% DOC instead of SDS yielded an almost identical CD spectrum (Supporting Information Figure 1A). C100 does not spontaneously adopt β-sheet structure but retains its α-helical conformation after incubation for 15 weeks at 4 °C when solubilized in SDS-containing buffer. CD together with SDS−PAGE analysis (Figure 1C,D) showed that in the presence of SDS at micelle-forming concentrations C100 precipitation was prohibited. MALDI-MS analysis of all protein bands excised from the SDS−PA gels verified the identity of C100 and the absence of bacterial protein contaminations (data not shown).

Labeling of C100 Cysteine Mutants for ESR Analysis. For ESR analyses the mutant L17C was used as it spontaneously formed dimers in living eukaryotic cells and could be processed by γ-secretase (*3*). Another cysteine mutant, F19C, which also spontaneously formed covalently linked dimers was expressed to study the effect of oligomerization mediated through a cysteine residue located on the opposite side of the α-helix. This allowed us to compare possible effects of the two different dimer interfaces.

As shown by SDS−PAGE analysis under nonreducing conditions, the cysteine mutants caused a shift toward the dimeric

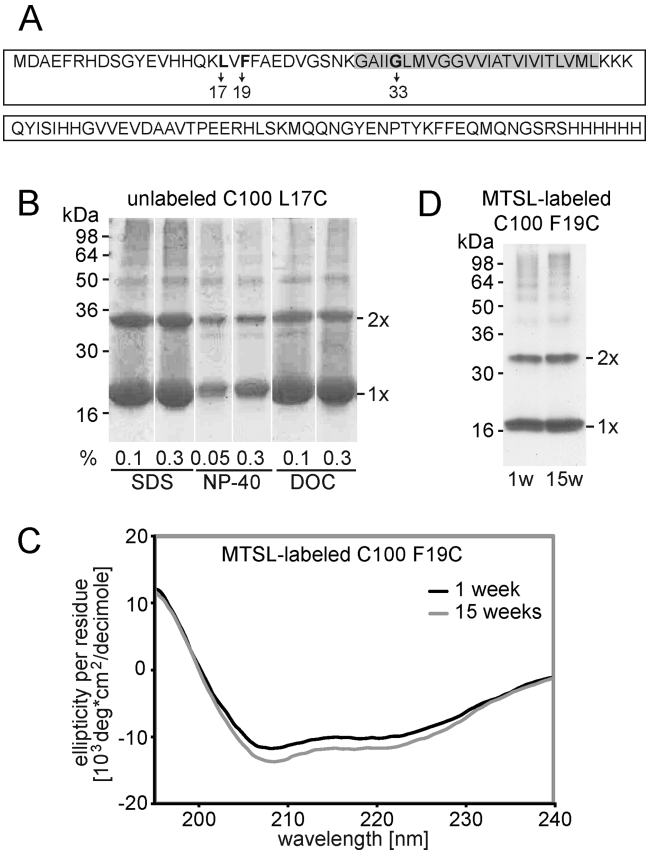

FIGURE 1: C100 is stable and structured in SDS-containing buffers. (A) Sequence of His-tagged C100. A gray box indicates membrane-embedded amino acid residues. Amino acids that are mutated are in bold, and numbering is according to the Aβ sequence. (B) Unlabeled C100 L17C (equal volumes) eluted from Ni-NTA columns, separated under nonreducing conditions on an SDS−PA gel and stained with Coomassie Brilliant Blue. All washing and elution buffers contained the indicated concentrations of the respective detergent. C100 monomers are indicated by 1x and dimers by 2x. (C) Circular dichroism (CD) spectra of C100 F19C in Tris/H_3PO_4 buffer. Samples were labeled with 10-fold molar excess of MTSL in the presence of 0.02 mM TCEP and 0.3% SDS and concentrated, and buffer was exchanged to Tris/H_3PO_4. The CD spectra show that C100 possesses an α-helical structure in SDS-containing buffer even after extended storage time. (D) C100 F19C at different time points of storage in Tris/H_3PO_4 buffer (w: week). Proteins were separated on an SDS−PA gel under nonreducing conditions and stained with Coomassie Brilliant Blue.

form due to covalent stabilization of the dimer compared to C100 wt (Figure 2B). This is in agreement with earlier publications where it was shown that in the presence of SDS C100 wt migrates predominantly as a monomer (*6*, *13*).

To permit spin labeling of C100 cysteine mutants for subsequent analysis of C100 oligomerization by ESR, possible disulfide bridges had to be reduced with TCEP (Figure 2A). TCEP is essentially nonreactive toward other functional groups and was added to the buffers used to solubilize protein from inclusion bodies, during the purification by Ni-NTA affinity chromatography, and during MTSL labeling (see Methods).

After removal of TCEP, C100 cysteine mutants treated with MTSL or untreated samples were stored for 24 h to permit reformation of disulfide bridges. Since in SDS−PA gels the majority of untreated C100 cysteine mutants migrated as dimers, which spontaneously formed after TCEP removal (Figure 2B, lanes −MTSL), the efficiency of the labeling reaction could be estimated from the monomer:dimer ratio of treated C100

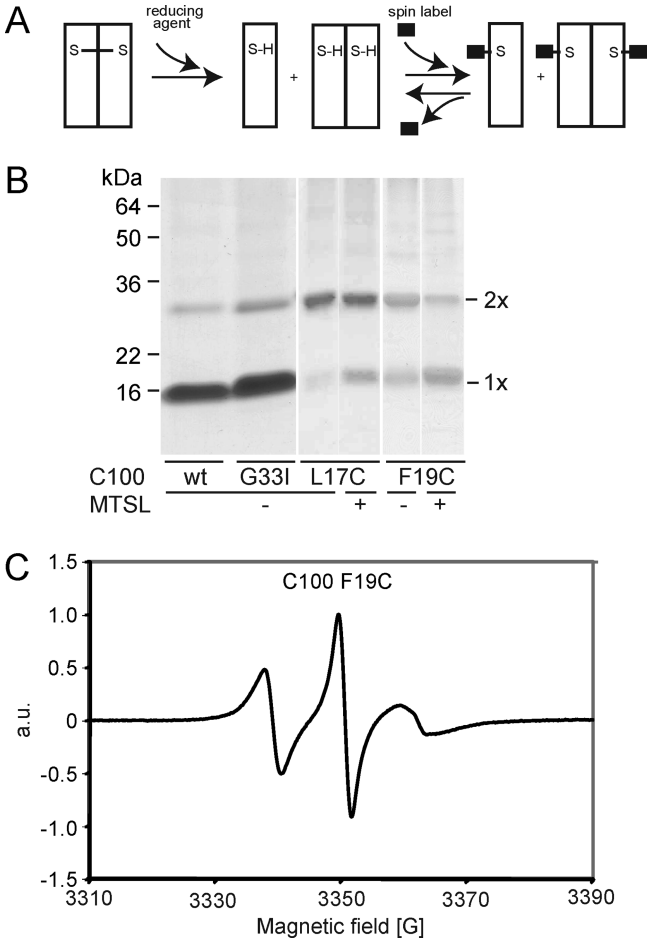

FIGURE 2: Labeling of C100 cysteine mutants. (A) Scheme of C100 spin labeling under reducing buffer conditions. C100 molecules are depicted as white rectangles; reduced cysteines are marked as SH and disulfide bridges as S−S. MTSL spin label is indicated by a small black square. S−S bridges are reduced by the addition of the reducing agent TCEP. Spin labeling prevents re-formation of disulfide bridges, thus leading to a high content of C100 monomers and residual amounts of noncovalent, SDS-stable dimers in the SDS−PA gels. C100 is stored under nonreducing conditions to prevent removal of the spin label from the protein. (B) C100 wt and mutants separated on an SDS−PA gel under nonreducing conditions and stained with Coomassie Brilliant Blue. Single cysteine mutants L17C and F19C were labeled with 10-fold MTSL excess (or buffer control) in the presence of 0.2 mM TCEP. C100 F19C shows a much stronger increase in monomer:dimer ratio after labeling than C100 L17C, indicating more efficient MTSL labeling. (C) cw-ESR spectrum of C100 F19C labeled with 10-fold MTSL excess in the presence of 0.02 mM TCEP and washed on a centrifugal filter device showing efficient labeling and removal of free spin label (au: arbitrary units).

(+MTSL) compared to the untreated proteins (−MTSL). High amounts of C100 migrating at the molecular weight of monomers indicated an efficient labeling reaction with the spin labeling reagent MTSL, which then prevented the reconstitution of disulfide bridges (Figure 2A,B, lanes +MTSL). This interpretation is valid under the assumption that MTSL-modified proteins are equally prone to forming SDS-resistant dimers compared to nonmodified C100.

Conditions were optimized for a maximum yield of labeled protein (see Supporting Information). Optimal C100 labeling and complete removal of free spin label for cw-ESR measurements were achieved with a 10-fold molar excess of MTSL in the presence of 0.02 mM TCEP (Supporting Information Figure 2, Figure 2C).

Incidently, we analyzed two other C100 mutants, G29C and S59C. G29C could not be spin labeled (data not shown), while S59C yielded ESR spectra similar to those of C100 F19C (Supporting Information Figure 2).

From the data shown in Figure 2B we conclude that the labeling reaction was much more efficient for the mutant F19C than for L17C, as increased amounts of MTSL-labeled F19C migrate as monomers compared to the unlabeled controls. Therefore, F19C was labeled for further studies using spin-labeled C100.

ESR Analysis of C100 Oligomerization. MTSL-labeled C100 F19C was analyzed by cw-ESR measurement to determine its oligomeric state. cw-ESR is used to study changes of labeled residues in their mobility and accessibility to water- or lipid-soluble paramagnetic quenchers. Here we used the technique to detect changes in samples containing varying concentrations of monomers, dimers, and cross-linked higher oligomers of C100 F19C. Oligomerization can cause a steric hindrance of the nitroxide movement, and the resulting lower mobility of the spin label would lead to alterations in the cw-ESR spectrum. Nitroxide label mobility is a major contributor to the rotational correlation time of the spin label, which is reflected by the line width in the cw-ESR spectrum (*14*). For C100 F19C, which has an α-helical conformation, a line broadening would indicate a steric inhibition of spin label movement upon cross-linking at a contact site close to the label.

C100 cross-linking with moderate amounts of the membrane-permeable reagent DFDNB showed that specific protein−protein interactions were almost completely restricted to preexisting dimers (Figure 3A, lane 5x DFDNB, 1d). We forced cross-linking of C100 molecules by extending the incubation time to 3 days in the presence of a 5-fold molar excess of DFDNB and by using extremely high concentrations of the reagent (Figure 3A, 20x and 50x DFDNB). Note that DFDNB lowered the apparent molecular weight of C100 in a concentration-dependent manner. This was not due to fragmentation of C100, as proved by MALDI-MS analysis (data not shown). We assume that this effect is caused by a decrease of the positive charge of the protein through DFDNB's reaction with amino groups.

Oligomers of C100 F19C generated by forced cross-linking (Figure 3A) were analyzed by CD measurement to determine whether oligomerization would impair native protein folding (Figure 3B). Interestingly, even a 50-fold molar excess of DFDNB did not affect the α-helical conformation of the protein. The slight differences observed in the spectra of the cross-linker-treated samples compared to nontreated C100 are most likely due to oligomerization. This is supported by the line broadening in the cw-ESR spectrum indicating decreased mobility of the spin label compared to the high mobility in the samples used as controls (Figure 3C). This change correlates with the presence and the amount of oligomers and is evident by the decrease of the maximum at ~3335 G and the shoulder appearing at ~3324 G (Figure 3C, right panel). Note that the maximum at ~3335 G, which is caused by the spin labels with the highest mobility, accounts for the greater part of the signal after cross-linking. This is explained by the fact that cross-linking reactions occur in a nonspecific manner and not only at sites close enough to the label to constrain its movement, most likely due to lateral diffusion and random collisions (*15*, *16*). Any influence that the cross-linking reagent might have on the spectra besides C100 oligomerization can be excluded since the line broadening in the ESR spectra was also seen when the concentration of the cross-linking reagent remained constant but the incubation

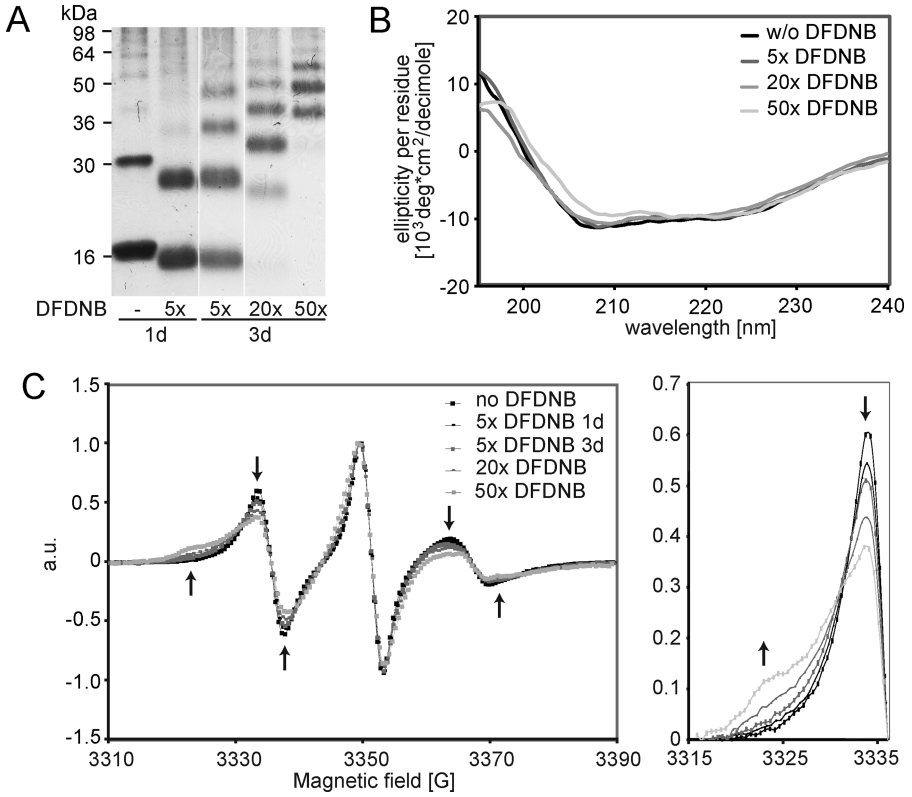

FIGURE 3: C100 does not form higher oligomers in 0.3% SDS. (A) DFDNB-cross-linked C100 F19C. Proteins were separated on an SDS−PA gel under reducing conditions and stained with Coomassie Brilliant Blue. C100 was labeled with a 10-fold MTSL excess in the presence of 0.02 mM TCEP. After buffer exchange to 50 mM sodium phosphate, cross-linking was performed with 5−50-fold molar excess of DFDNB at room temperature for 30 min. Samples were stored at 4 °C for 1 or 3 days as indicated. (B) CD spectra of C100 F19C 3 days after cross-linking with DFDNB. Samples are identical to (A). Cross-linking does not change the α-helical conformation of C100. (C) cw-ESR spectra of C100 F19C after cross-linking with DFDNB. Samples are identical to (A) and (B). For better resolution, the 3315−3336 G section of the spectrum is shown enlarged in the right panel. Increasing formation of trimers and higher oligomers by the cross-linking reaction reduces the mobility of the spin label, as indicated by a lowering of the peak at 3334 G and the appearance of a shoulder around 3324 G as well as further alterations in the spectrum (marked by arrows) (au: arbitrary units).

time was prolonged (Figure 3C, 5x DFDNB, 1d vs 3d). Also note that the change in line shape is already detected after a 1 day treatment with a 5-fold molar excess of DFDNB, which merely promotes the formation of C100 dimers and causes the appearance of a faint band migrating at the molecular weight of trimers.

There was no gross difference between the ESR spectra of C100 F19C prepared in the presence of 0.1% DOC versus 0.3% SDS (Supporting Information Figure 1B) or between C100 L17C versus F19C (Supporting Information Figure 3). This indicates that the oligomerization state determined here does not depend on the specific detergent used or on which of the two dimer interfaces is used by the cysteine mutants.

We conclude that C100 is normally present only in the form of monomers and dimers but not higher oligomers and that the preservation of the α-helical structure is independent of the oligomerization state. This strongly indicates an unusually high conformational stability of SDS-treated C100.

GSM Binding to C100 Analyzed by SPR and Molecular Modeling. Previously, we have suggested that the decreased production of Aβ42 peptides and the concomitant increase of Aβ38 modulated by sulindac sulfide are mediated through direct binding of the GSM to the Aβ sequence. This compound showed a rapid association and dissociation in a BIAcore analysis of its interaction with Aβ in contrast to its sulfone derivative, which only differs from sulindac sulfide in the oxidation state of the sulfur atom (*11*). Here, we used the full-length γ-secretase substrate C100 to test the interaction with sulindac sulfide.

C100 variants were immobilized through their C-terminal His tag to a Ni-charged NTA SPR sensor chip, and sulindac sulfide and its sulfone derivative were injected onto C100 surfaces. Upon sulindac sulfide injection onto C100 wt, a rapid increase in response occurred in a concentration-dependent manner, followed by a rapid return to baseline at the end of the injection, indicating fast association and dissociation rates similar to previously tested Aβ (Figure 4A (*11*)). In contrast, sulindac sulfone injection did not increase the response significantly (Figure 4B). Next, sulindac sulfide binding to the C100 mutants L17C and G33I was analyzed by SPR. We found that sulindac sulfide bound in a concentration-dependent manner to both mutants G33I and L17C (Supporting Information Figure 4). However, the overlay of response curves of C100 L17C and G33I revealed that at the highest concentration of sulindac sulfide (50 μM) injected the maximum response was increased by 29% for C100 L17C, while binding to C100 G33I was attenuated by 25% when normalized to the amount of C100 coupled to the sensor chip and compared to C100 wt (Figure 4C,D). Considering that the monomer:dimer ratio of the mutant G33I was identical to that of the wild type in an SDS−PA gel (see Figure 2B) while L17C showed increased dimerization, the SPR measurements may indicate that sulindac sulfide preferentially binds to C100 dimers. An isoleucine at position 33 could directly interfere with binding. A visual inspection of the SPR sensorgrams indicates that both association and dissociation of sulindac sulfide from C100 L17C are somewhat slower compared to C100 wt

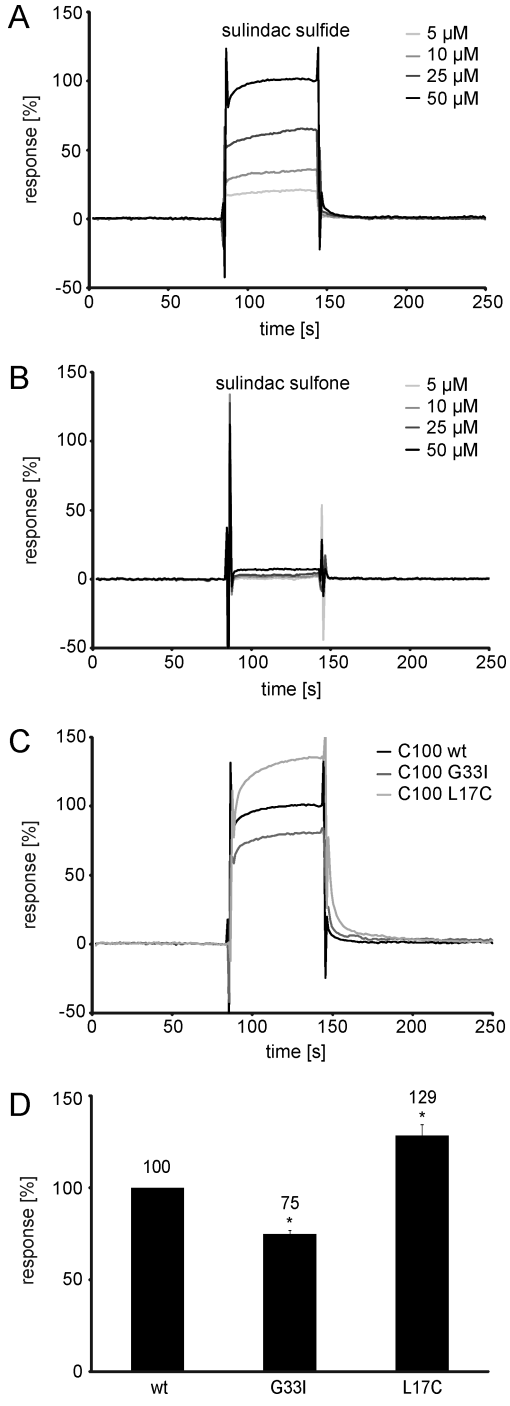

FIGURE 4: SPR analysis of sulindac sulfide binding to C100. (A−C) Interaction of sulindac sulfide with C100 determined by SPR analysis. Overlays of representative SPR sensorgrams obtained from injections of sulindac sulfide (A, C) or sulindac sulfone (B) onto C100 wt (A, B, C) or mutants L17C and G33I (C) Ni-NTA sensor chip surfaces. Compounds at 50 μM (C) or at indicated concentrations were injected for 60 s at a flow rate of 30 μL/min. All binding curves were double-reference subtracted from DMSO buffer blank and the reference flow cell and adjusted to the molecular weight of the compounds. Sensorgrams shown are the mean of three (A, B) or four (C) independent measurements. Binding of 50 μM sulindac sulfide to C100 wt is set as 100%, with binding to C100 L17C or G33I normalized to the response of C100 coupling. (D) Binding of sulindac sulfide to C100 wt and mutants assessed for significance. Values were calculated from sensorgrams averaged in (C). *, $p < 0.05$.

(Figure 4C). Unfortunately, association and dissociation rates of such small molecules are too fast to allow detailed kinetic analyses.

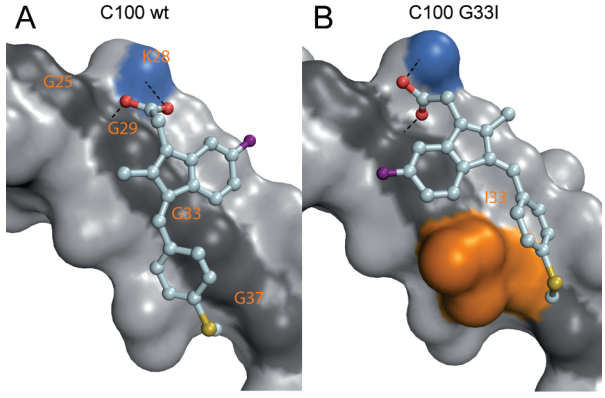

FIGURE 5: Model of sulindac sulfide flexibly docked to the APP-TMS of C100 wt (A) and G33I (B) mutant. The GSM is rotated by 180° around its longitudinal axis in the mutant compared to the wt structure and laterally shifted away from position 33. Extensive van der Waals contacts are formed between I33 and sulindac sulfide, restricting the vibrational and translational freedom of this side chain. Oxygen atoms are depicted in red, sulfur atoms in yellow, and fluorine atoms in purple. The glycine residues that form the flat binding surface are depicted in dark gray; K28 and I33 side chains are colored blue and orange, respectively. Potential hydrogen bonds are indicated as black dashed lines.

We further aimed to better characterize the sulindac sulfide binding site by molecular modeling. The binding site has been indicated earlier to lie on the dimer interface formed by the three consecutive GxxxG motifs in the APP-TMS, with a preferred binding site between glycine residues 29 and 33 (Figure 5A (*11*)). The bulky side chain of isoleucine in position 33 intersects the flat and continuous binding site (Figure 5B). Therefore, sulindac sulfide binding to C100 G33I differs from its binding to C100 wt. Although the same hydrogen bonds between C100 G33I and sulindac sulfide are detected by flexible docking of this compound by means of GOLD (see Methods), compared to the C100 wt structure sulindac sulfide is rotated by 180° around its longitudinal axis and laterally shifted by about 5 Å in the mutant. This prevents clashes with isoleucine 33. According to the model, sulindac sulfide would intercalate between the bulky side chains of residues I32, I33, and L36 forming extensive van der Waals contacts and thereby reduce the motion of side chains, particularly I33. The resulting loss in entropy could explain the 25% reduction in the SPR response for the G33I mutant.

DISCUSSION

By studying the properties of purified C100 expressed in *E. coli* we found that the protein is highly stable, has an α-helical conformation, and is mostly present as monomers and dimers.

Spin labeling of C100 cysteine mutants revealed a difference in labeling efficiency for the mutations L17C and F19C which are located on opposite sides of a presumed α-helix. F19C labeling was much more efficient, likely because C100 dimerization via the triple GxxxG motif in the TMS would place cysteines at position 17 (~2 helix turns away from the first GxxxG contact site at glycine 25) on the dimer interface, favoring disulfide bridge formation, while cysteines at position 19 (~1.5 helix turns) would be located off the interface. We assume that both mutants react equally well with MTSL but that L17C is more prone to re-forming disulfide bridges spontaneously during the washing steps before complete TCEP removal.

By CD measurement we could verify that C100 samples possessed an α-helical conformation. Surprisingly, an α-helical

conformation was also observed for cross-linked C100 samples that were forced to form covalently linked higher oligomers (Figure 3B), as opposed to engineered dimers of the Aβ sequence that generally have an increased β-sheet content (*17*). This indicates that, unlike the Aβ peptide, C100 dimers are not per se prone to β-sheet conversion or to further aggregation when prepared in the presence of SDS. In an earlier study, NMR analyses identified C100 as monodisperse in LMPG micelles when complexation of GSMs with purified C100 was investigated. It was claimed that even dilute C100 was present only in the form of very high molecular weight aggregates (*12*). In contrast, we show by cw-ESR that C100 purified as described is neither specifically prone to aggregation nor to forming higher oligomers and that monomers and dimers are highly stable. Only when stored for several weeks, marginal loss of protein by precipitation occurred, but any C100 that remained in solution had retained its α-helical conformation (Figure 1C). Thus, our findings do not conflict with earlier studies showing that C100 fibril formation can occur under denaturing conditions (*18*). In summary, our purification protocol is suitable for the production of pure C100 molecules with the expected biophysical characteristics as required for γ-secretase *in vitro* studies. By allowing researchers to monitor oligomerization, cw-ESR has the potential to improve widely used *in vitro* studies with C100 aimed at better understanding the molecular details of the γ-secretase cleavage mechanism.

Earlier studies have identified the TMS of C100 not only as a site for self-interaction through the GxxxG motif (*3*) but also for binding of GSMs which thereby modulate Aβ production in cellular assays (*10*, *11*). Here we show by SPR analysis that the GSM sulindac sulfide binds specifically and in a concentration-dependent manner to C100. Since GSMs were shown to act by disturbing the dimer interface of C100 (*11*), we compared the maximum rate of response upon sulindac sulfide binding between C100 G33I which has an increased monomer:dimer ratio in the absence of SDS (*3*), monomeric/dimeric C100 wt, and the engineered dimer L17C. Response was higher for L17C, which indicates that sulindac sulfide binds more strongly to dimers than to monomers. This suggests that in addition to preventing dimerization GSMs may act via the disruption of existing C100 dimers. A visual inspection of the curve implies that both association and dissociation of sulindac sulfide to C100 L17C are slower, possibly due to the covalent linkage that restricts C100 movement.

We performed a flexible docking analysis to find an explanation for the diminished maximum response yielded by sulindac sulfide binding to G33I (Figure 4C,D). Previously, we reported that the flat surface provided by the four glycine residues, G25, G29, G33, and G37, provides an optimal flat and rigid binding interface for the GSMs (*11*). Flexible docking of sulindac sulfide to C100 G33I now indicates that GSMs have the property of adapting themselves geometrically to differently formed binding sites. Rotation by 180° and lateral shifting of the compound even permit the formation of the same hydrogen-bonding patterns as observed in the wt structure, where a continuous flat binding site is preserved. Comparison with the wt complex reveals that no additional torsional constraints are imposed on the aromatic ring system of sulindac sulfide. The extensive van der Waals contacts formed between the aromatic ring system and I33 are therefore likely to increase the overall binding enthalpy. However, this effect is very likely countervailed by a dramatic loss in entropy, because the vibrational and translational freedom of the isoleucine side chain will be significantly restricted upon binding of sulindac sulfide (*19*). Therefore, sulindac sulfide is expected to bind with a reduced affinity to the G33I mutant compared to C100 wt.

These results strengthen previous reports by us and others (*10*, *11*) that GSM binding to the APP-TMS is specific and can be assigned to the dimer interface formed by the triple GxxxG motif of the C100-TMS. The interaction most likely does not depend on the precise primary sequence but on the α-helical conformation and is promoted by a flat helix surface such as provided by the GxxxG motif. The fact that sulindac sulfide binding to C100 G33I is impaired implies that the GxxxG surface must be conserved for optimal GSM binding. In cell membranes, GSMs would bind to both C100 monomers and dimers, either inhibiting dimerization of monomers or monomerizing preformed dimers. This may explain mechanistically how GSMs can modulate the ratio of Aβ42 to Aβ38 in the consecutive γ-secretase cleavage process in living cells.

ACKNOWLEDGMENT

We thank Prof. Christian Haass and Prof. Harald Steiner (LMU Munich) for kindly providing the pQE60-C100 construct.

SUPPORTING INFORMATION AVAILABLE

Four figures containing additional data and captions. This material is available free of charge via the Internet at http://pubs.acs.org.

REFERENCES

1. Kaden, D., Munter, L. M., Joshi, M., Treiber, C., Weise, C., Bethge, T., Voigt, P., Schaefer, M., Beyermann, M., Reif, B., and Multhaup, G. (2008) Homophilic interactions of the amyloid precursor protein (APP) ectodomain are regulated by the loop region and affect beta-secretase cleavage of APP. *J. Biol. Chem. 283*, 7271–7279.
2. Wang, Y., and Ha, Y. (2004) The X-ray structure of an antiparallel dimer of the human amyloid precursor protein E2 domain. *Mol. Cell 15*, 343–353.
3. Munter, L. M., Voigt, P., Harmeier, A., Kaden, D., Gottschalk, K. E., Weise, C., Pipkorn, R., Schaefer, M., Langosch, D., and Multhaup, G. (2007) GxxxG motifs within the amyloid precursor protein transmembrane sequence are critical for the etiology of Abeta42. *EMBO J. 26*, 1702–1712.
4. Harmeier, A., Wozny, C., Rost, B. R., Munter, L. M., Hua, H., Georgiev, O., Beyermann, M., Hildebrand, P. W., Weise, C., Schaffner, W., Schmitz, D., and Multhaup, G. (2009) Role of amyloid-beta glycine 33 in oligomerization, toxicity, and neuronal plasticity. *J. Neurosci. 29*, 7582–7590.
5. Rutten, B. P., Wirths, O., Van de Berg, W. D., Lichtenthaler, S. F., Vehoff, J., Steinbusch, H. W., Korr, H., Beyreuther, K., Multhaup, G., Bayer, T. A., and Schmitz, C. (2003) No alterations of hippocampal neuronal number and synaptic bouton number in a transgenic mouse model expressing the beta-cleaved C-terminal APP fragment. *Neurobiol. Dis. 12*, 110–120.
6. Beel, A. J., and Sanders, C. R. (2008) Substrate specificity of gamma-secretase and other intramembrane proteases. *Cell. Mol. Life Sci. 65*, 1311–1334.
7. Munter, L. M., Botev, A., Richter, L., Hildebrand, P. W., Althoff, V., Weise, C., Kaden, D., and Multhaup, G. (2010) Aberrant APP processing in hereditary forms of Alzheimer disease can be rescued by mutations in the APP GxxxG motif. *J. Biol. Chem. 285*, 21636–21643.
8. Eriksen, J. L., Sagi, S. A., Smith, T. E., Weggen, S., Das, P., McLendon, D. C., Ozols, V. V., Jessing, K. W., Zavitz, K. H., Koo, E. H., and Golde, T. E. (2003) NSAIDs and enantiomers of flurbiprofen target gamma-secretase and lower Abeta 42 in vivo. *J. Clin. Invest. 112*, 440–449.
9. Weggen, S., Eriksen, J. L., Das, P., Sagi, S. A., Wang, R., Pietrzik, C. U., Findlay, K. A., Smith, T. E., Murphy, M. P., Bulter, T., Kang, D. E., Marquez-Sterling, N., Golde, T. E., and Koo, E. H. (2001) A subset of NSAIDs lower amyloidogenic Abeta42 independently of cyclooxygenase activity. *Nature 414*, 212–216.

10. Kukar, T. L., Ladd, T. B., Bann, M. A., Fraering, P. C., Narlawar, R., Maharvi, G. M., Healy, B., Chapman, R., Welzel, A. T., Price, R. W., Moore, B., Rangachari, V., Cusack, B., Eriksen, J., Jansen-West, K., Verbeeck, C., Yager, D., Eckman, C., Ye, W., Sagi, S., Cottrell, B. A., Torpey, J., Rosenberry, T. L., Fauq, A., Wolfe, M. S., Schmidt, B., Walsh, D. M., Koo, E. H., and Golde, T. E. (2008) Substrate-targeting gamma-secretase modulators. *Nature 453*, 925–929.
11. Richter, L., Munter, L. M., Ness, J., Hildebrand, P. W., Dasari, M., Unterreitmeier, S., Bulic, B., Beyermann, M., Gust, R., Reif, B., Weggen, S., Langosch, D., and Multhaup, G. (2010) Amyloid beta 42 peptide (Aβ42)-lowering compounds directly bind to Aβ and interfere with amyloid precursor protein (APP) transmembrane dimerization. *Proc. Natl. Acad. Sci. U.S.A. 107*, 14597–14602.
12. Beel, A. J., Barrett, P., Schnier, P. D., Hitchcock, S. A., Bagal, D., Sanders, C. R., and Jordan, J. B. (2009) Nonspecificity of binding of gamma-secretase modulators to the amyloid precursor protein. *Biochemistry 48*, 11837–11839.
13. Dyrks, T., Dyrks, E., Masters, C., and Beyreuther, K. (1992) Membrane inserted APP fragments containing the beta A4 sequence of Alzheimer's disease do not aggregate. *FEBS Lett. 309*, 20–24.
14. Hubbell, W. L., Cafiso, D. S., and Altenbach, C. (2000) Identifying conformational changes with site-directed spin labeling. *Nat. Struct. Biol. 7*, 735–739.
15. Frye, L. D., and Edidin, M. (1970) The rapid intermixing of cell surface antigens after formation of mouse-human heterokaryons. *J. Cell Sci. 7*, 319–335.
16. Kiehm, D. J., and Ji, T. H. (1977) Photochemical cross-linking of cell membranes. A test for natural and random collisional cross-links by millisecond cross-linking. *J. Biol. Chem. 252*, 8524–8531.
17. Schmechel, A., Zentgraf, H., Scheuermann, S., Fritz, G., Pipkorn, R., Reed, J., Beyreuther, K., Bayer, T. A., and Multhaup, G. (2003) Alzheimer beta-amyloid homodimers facilitate A beta fibrillization and the generation of conformational antibodies. *J. Biol. Chem. 278*, 35317–35324.
18. Tjernberg, L. O., Naslund, J., Thyberg, J., Gandy, S. E., Terenius, L., and Nordstedt, C. (1997) Generation of Alzheimer amyloid beta peptide through nonspecific proteolysis. *J. Biol. Chem. 272*, 1870–1875.
19. Lee, A. L., Kinnear, S. A., and Wand, A. J. (2000) Redistribution and loss of side chain entropy upon formation of a calmodulin-peptide complex. *Nat. Struct. Biol. 7*, 72–77.